Progress In Electromagnetics Research, Vol. 142, 743–770, 2013

PARAMETER SELECTION AND ACCURACY IN TYPE-3 NON-UNIFORM FFTS BASED ON GAUSSIAN GRIDDING

Amedeo Capozzoli*, Claudio Curcio, Angelo Liseno, and Antonio Riccardi

Dipartimento di Ingegneria Elettrica e delle Tecnologie dell'Informazione, Università di Napoli Federico II, via Claudio 21, Napoli I 80125, Italy

Abstract—We provide a sufficient condition to select the parameters of Type 3 Non-Uniform Fast Fourier Transform (NUFFT) algorithms based on the Gaussian gridding to fulfill a prescribed accuracy. This is a problem of significant interest in many areas of applied electromagnetics, as for example fast antenna analysis and synthesis and fast calculation of the scattered fields, as well as in medical imaging comprising ultrasound tomography, computed axial tomography, positron emission tomography and magnetic resonance imaging. The approach is related to the one dimensional case and follows the work in [15]. The accuracy of the proposed choice is first numerically assessed and then compared to that achieved by the approach in [2]. The convenience of the strategy devised in this paper is shown. Finally, the use of the Type 3 NUFFT is highlighted for an electromagnetic application consisting of the implementation of the aggregation and disaggregation steps in the fast calculation of the scattered field by the Fast Multipole Method.

1. INTRODUCTION

In a large number of numerical problems of electromagnetics, the need arises of evaluating Non-Uniform Discrete Fourier Transforms (NUDFTs), namely DFTs with data and/or results on irregular grids. Examples concern imaging [1–3], solutions to differential and integral equations [4–7], fast array antenna analysis [8] and

Received 24 July 2013, Accepted 7 September 2013, Scheduled 16 October 2013
* Corresponding author: Amedeo Capozzoli (a.capozzoli@unina.it).

synthesis [9] and antenna diagnosis [10], to mention just a few. Concerning the first mentioned topic, calculating NUDFTs is particularly relevant in medical imaging, as for instance ultrasound tomography [11], Computed Axial Tomography (CAT) [12], Positron Emission Tomography (PET) [13] or Magnetic Resonance Imaging (MRI) [14], for which the fast and accurate calculation of diagnostic images is the main issue to be addressed.

To calculate the NUDFTs, it is unfortunately not possible to promptly exploit the computational benefit ($O(N \log N)$ complexity) of standard Fast Fourier Transforms (FFTs) which on the contrary require Cartesian input and output grids. This solicited the development of Non-Uniform FFT (NUFFT) algorithms capable to perform accurate computations essentially with $O(N \log N)$ complexity. NUFFTs exploit the computational benefit of standard FFTs by fast and accurate pre- and/or post-interpolation stages, properly tailored to the problem at hand, from/to regular to/from irregular grids. The various proposed NUFFT algorithms then differentiate by the specific trade-off between accuracy and computational burden [15–19].

One of the many proposed NUFFT algorithms employ Gaussian windows to interpolate "non-uniformly sampled" exponentials by finite summations of "uniformly sampled" ones, a technique known as "Gaussian gridding". Error bounds for the accuracy of those interpolations have been thoroughly examined in [15] and NUFFT algorithms for the "Type 1" (transforms from irregular to regular grids), "Type 2" (transforms from regular to irregular grids) and "Type 3" (transforms from irregular to irregular grids) problems have been described. However, in [15], the selection of the algorithms parameters (support of the employed Gaussian windows, number of interpolation samples etc.) has not been investigated.

Subsequently, a fast way to implement Gaussian gridding, addressed to as "fast Gaussian gridding", has been proposed for the Type 1 and 2 problems in [19] and for the Type 3 problem in [2]. This time the Authors of [2, 19] give indications on the choice of the relevant algorithm parameters but:

- They do not provide analytical justifications and refer the Reader to [15] which however does not discuss, as mentioned, the parameters selection;
- For the Type 3 problem, the suggested choices can lead to inconsistent or poor results;
- The parameters choice is independent of the target accuracy.

Purpose of this paper is to provide and show the convenience of a criterion for the parameters choice with reference to Gaussian

gridding applied to the Type 3 problem in the one dimensional case. In particular, by exploiting the results in [15], we provide a sufficient condition to select the parameters of Type 3 Non-Uniform Fast Fourier Transform (NUFFT-3) algorithms based on the Gaussian gridding to fulfill a prescribed accuracy in the computation of the NUDFT.

The paper is organized as follows. Section 2 is devoted to recall the NUFFT-3 scheme based on Gaussian gridding and illustrated in [2]. Section 3 presents general conditions that must be satisfied by the algorithm parameters. In Section 4, the results of [15] are exploited to derive those conditions on the relevant parameters to achieve a prefixed accuracy. The parameters choice to fulfill the mentioned accuracy is analytically worked out in Section 5. Section 6 presents numerical results aimed at proving the accuracy of the NUFFT-3 scheme under the parameters choice of Section 5 and, in that section, the results are compared to those achieved by the parameters choice suggested in [2] and the main issues of such an approach are also highlighted. In Section 7, the fruitful use of the NUFFT-3 is shown for an electromagnetic application consisting of the implementation of the aggregation and disaggregation steps in the fast calculation of the scattered field by the Fast Multipole Method (FMM) [7]. Finally, conclusions follow in Section 8.

2. TYPE 3 NON-UNIFORM FFT

In this section, we briefly recall the 1D Type 3 NUDFT (NUDFT-3) and shortly outline the related NUFFT-3 algorithm developed in [2]. For the reader's convenience, this section is divided in six subsections, the first one for the NUDFT-3 and the other five describing each of the five steps involved in the NUFFT-3.

2.1. NUDFT-3 and NUFFT-3

Let $\{x_i\}_{i=0}^{N-1}$ be a set of N non equispaced points, $\{f_i\}_{i=0}^{N-1}$ a set of corresponding coefficients and $\{s_k\}_{k=0}^{N_s-1}$ a set of N_s non-equispaced angular frequencies. The transformation

$$F_k = \sum_{i=0}^{N-1} f_i e^{-js_k x_i} \quad k = 0, \ldots, N_s - 1 \tag{1}$$

is referred to as a NUDFT-3 [2].

As a first step towards the NUFFT-3 based on Gaussian gridding, we observe that the values $\{F_k\}_{k=0}^{N_s-1}$ in Eq. (1) can be regarded as the

samples of the continuous Fourier Transform $F_\delta(s)$ of $f_\delta(x)$ defined as

$$f_\delta(x) = \sqrt{2\pi} \sum_{i=0}^{N-1} f_i \delta(x - x_i), \tag{2}$$

i.e.,

$$F_\delta(s) = \frac{1}{\sqrt{2\pi}} \int_{-\infty}^{\infty} f_\delta(x) e^{-jsx} dx. \tag{3}$$

Accordingly and roughly speaking, the idea behind the NUFFT-3 is that of interpolating the samples $\{f_i\}_{i=0}^{N-1}$ from the non-uniform lattice $\{x_i\}_{i=0}^{N-1}$ to a uniform one by convolving $f_\delta(x)$ with a smoothing window $g_\tau(x)$, employing a standard FFT to obtain spectral samples on a uniform grid and finally interpolating such spectral samples to the non-uniform grid $\{s_k\}_{k=0}^{N_s-1}$ by convolving the result with a proper window $g_\sigma(s)$. It should be remarked that the windows employed for the spatial and spectral interpolations should be properly compensated. The interpolations being convolutions and by exploiting the properties of the Fourier transform, the spectral window $g_\sigma(s)$ is compensated in the spatial domain through its inverse Fourier transform $G_\sigma(x)$ prior to the application of the standard FFT, while the spatial window $g_\tau(x)$ is compensated in the spectral domain through its Fourier transform $G_\tau(x)$ following the interpolation of the uniform samples achieved by the standard FFT to the non-uniform grid of interest.

More in detail, the interpolation from the non-uniform lattice $\{x_i\}_{i=0}^{N-1}$ to a uniform one to be determined, say $\{n\Delta x\}_{n=-M_r/2}^{M_r/2-1}$ (assuming M_r even), is obtained by convolving $f_\delta(x)$ with $g_\tau(x)$ as

$$f_\tau(x) = f_\delta(x) \star g_\tau(x) = \frac{1}{\sqrt{2\pi}} \int_{-\infty}^{\infty} f_\delta(x') g_\tau(x - x') dx' = \sum_{i=0}^{N-1} f_i g_\tau(x - x_i). \tag{4}$$

As mentioned and prior to be transformed, $f_\tau(x)$ is multiplied by the reciprocal of $G_\sigma(x)$, namely

$$f_\tau^{-\sigma}(x) = \frac{f_\tau(x)}{G_\sigma(x)}. \tag{5}$$

Applying the standard FFT to the uniform samples of $f_\tau^{-\sigma}(x)$ enables calculating its continuous Fourier transform $F_\tau^{-\sigma}(s)$ on a uniform grid to be determined, say $\{m\Delta s\}_{m=-M_r/2}^{M_r/2-1}$.

After that, and by virtue of Eq. (5), the values $\{F_\tau(s_k)\}_{k=0}^{N_s-1}$ can be recovered by convolving $F_\tau^{-\sigma}(s)$ with $g_\sigma(s)$ as follows

$$F_\tau(s) = \left[F_\tau^{-\sigma}(s) \star g_\sigma(s)\right] = \frac{1}{\sqrt{2\pi}} \int_{-\infty}^{+\infty} F_\tau^{-\sigma}\left(s'\right) g_\sigma\left(s - s'\right) ds'. \quad (6)$$

Finally, the spatial interpolation window can be compensated.

In the framework of this general scheme, Gaussian gridding consists of using Gaussian bell functions as spatial and spectral interpolation windows, namely $g_\tau(x) = e^{-x^2/(4\tau)}$ and $g_\sigma(s) = e^{-s^2/(4\sigma)}$, having corresponding transforms $G_\tau(s) = \sqrt{2\tau}e^{-\tau s^2}$ and $G_\sigma(x) = \sqrt{2\sigma}e^{-\sigma x^2}$, respectively.

In the following, the five steps necessary to carry out the NUFFT-3 based on Gaussian gridding are briefly summarized.

2.2. Step #1: Gaussian Gridding in the Spatial Domain

The first step is an application of Eq. (4), that is

$$f_\tau(n\Delta x) = \sum_{i=0}^{N-1} f_i e^{-\frac{(n\Delta x - x_i)^2}{4\tau}}, \quad n = -M_r/2, \ldots, (M_r - 1)/2. \quad (7)$$

Due to the rapid decay of $g_\tau(x)$, f_i significantly contributes to only few samples of $f_\tau(n\Delta x)$. In particular, on defining $\mathrm{Int}[\alpha]$ the nearest integer to α, by letting $\zeta_i = \mathrm{Int}[x_i/\Delta x]$, $i = 0, \ldots, (N-1)$, denote the nearest regular grid point to $x_i/\Delta x$ and assigning $n' = n - \zeta_i$, the contributions of each coefficient f_i to $f_\tau(n\Delta x)$ can be ignored when $|n'| > m_{sp}$, where m_{sp} is a parameter properly selected according to the required accuracy.

2.3. Step #2: Pre-compensating for the Interpolation Window Involved by the Gaussian Gridding in the Spectral Domain

This step is an application of Eq. (5), i.e.,

$$f_\tau^{-\sigma}(n\Delta x) = \frac{1}{\sqrt{2\sigma}} e^{\sigma(n\Delta x)^2} f_\tau(n\Delta x), \quad n = -M_r/2, \ldots, M_r/2-1. \quad (8)$$

2.4. Step #3: Standard FFT

A standard FFT is applied to the samples of $f_\tau^{-\sigma}(x)$ to provide

$$F_\tau^{-\sigma}(m\Delta s) \simeq \frac{\Delta x}{\sqrt{2\pi}} \sum_{n=-M_r/2}^{M_r/2-1} f_\tau^{-\sigma}(n\Delta x) e^{-jmn\Delta x\Delta s}. \quad (9)$$

2.5. Step #4: Gaussian Gridding in the Spectral Domain

Step #4 is an application of Eq. (6), that is

$$F_\tau(s_k) = \frac{\Delta s}{\sqrt{2\pi}} \sum_{m=-M_r/2}^{M_r/2-1} F_\tau^{-\sigma}(m\Delta s) e^{-\frac{(m\Delta s - s_k)^2}{4\sigma}}. \tag{10}$$

Similarly to Step #1, due to the rapid decay of $g_\sigma(s)$, $F_\tau^{-\sigma}(m\Delta s)$ significantly contributes to only few samples of $F_\tau(s_k)$. In particular, on letting $\eta_k = Int[s_k/\Delta s]$, $k = 0, \ldots, (N_s - 1)$, and $m' = m - \eta_k$, the contributions of each coefficient $F_\tau^{-\sigma}(m\Delta s)$ can be ignored when $|m'| > m_{sp}$ which, in the approach of [2], is the same as that involved in the spatial domain Gaussian gridding thanks to the relationship between Δx and Δs due to the application of the standard FFT.

2.6. Step #5: Post-compensating for the Interpolation Window Involved by the Gaussian Gridding in the Spatial Domain

This Step consists of compensating the initial smoothing in Eq. (4), namely,

$$\bar{F}(s_k) = \frac{1}{\sqrt{2\tau}} e^{\tau s_k^2} F_\tau(s_k), \tag{11}$$

so obtaining the computed $\bar{F}(s_k)$ approximating the F_k's in Eq. (1).

3. GENERAL CONDITIONS

According to the foregoing section, the algorithm parameters (APs) to be chosen are

- The number of spatial and spectral uniform sampling points M_r;
- The parameter τ of the spatial Gaussian bell interpolating function;
- The parameter σ of the spectral Gaussian bell interpolating function;
- The number of $2m_{sp}$ significant samples of the spectral and spatial Gaussian interpolating functions;
- The sampling step Δx in the spatial domain;
- The sampling step Δs in the spectral domain.

In this section, we derive the conditions, required by the different steps of the algorithm, that must be satisfied by the APs. We also indicate proper pre- and post-processing steps to reduce the number

of spatial and spectral uniform sampling points M_r.

Condition #1

In Step #2, the support of $1/G_\sigma(x)$ is unbounded, while that of $f_\tau(x)$ is essentially bounded, being $f_\tau(x)$ the sum of Gaussian functions having negligible values for $|x - x_i|$ a few times larger than the corresponding standard deviations. Therefore,

$$\sigma < \frac{1}{4\tau} \tag{12}$$

is required to ensure that the support of $f_\tau^{-\sigma}(x)$ is bounded and essentially determined by that of $f_\tau(x)$.

Condition #2

To accurately performing Step #3, M_r and Δx should be chosen so that the interval $[-(M_r/2)\Delta x, (M_r/2-1)\Delta x]$ contain most of the entire signal energy in agreement with the desired accuracy.

The interval $[x^{\min} - m_{sp}\Delta x, x^{\max} + m_{sp}\Delta x]$, with $x^{\min} = \min\{x_i\}_{i=0}^{N-1}$ and $x^{\max} = \max\{x_i\}_{i=0}^{N_s-1}$, must be then the smallest interval containing the support of $f_\tau^{-\sigma}(x)$. Therefore, Condition #2 requires, apart from the asymmetry issues to be discussed in Subsection 3.1, that

$$\frac{M_r}{2} \geq \frac{X}{\Delta x} + m_{sp}, \tag{13}$$

where $X = \max\{|x^{\min}|, |x^{\max}|\}$.

Condition #3

To avoid aliasing in Step #3, the space sampling step Δx must satisfy the Nyquist sampling condition

$$\Delta x \leq \frac{\pi}{B_s} \tag{14}$$

where B_s is the spatial bandwidth of $f_\tau^{-\sigma}(x)$.

Condition #4

The spatial and spectral sampling steps and the uniform samples number M_r must satisfy the FFT condition

$$\Delta s = \frac{2\pi}{\Delta x M_r}. \tag{15}$$

Condition #5

Similarly to Condition #2, to accurately perform the calculation of the integral in Eq. (10), the interval $[-(M_r/2)\Delta s, ((M_r-1)/2)\Delta s]$ must capture most of the energies of the integrands $\{F_\tau^{-\sigma}(s')g_\sigma(s_k-s')\}_{k=0}^{N_s-1}$.

The interval $[s^{\min} - m_{sp}\Delta s, s^{\max} + m_{sp}\Delta s]$, with $s^{\min} = \min\{s_k\}_{k=0}^{N_s-1}$ and $s^{\max} = \max\{s_k\}_{k=0}^{N_s-1}$, must be then the smallest interval containing the supports of $F_\tau^{-\sigma}(s')g_\sigma(s_k-s')$, $k=0,\ldots,N_s-1$, taken as functions of s'. Therefore, Condition #5 requires that

$$\frac{M_r}{2} \geq \frac{S}{\Delta s} + m_{sp}, \tag{16}$$

where $S = \max\{|s^{\min}|, |s^{\max}|\}$.

3.1. Centering of the Spatial and Spectral Grids

To speed up the computations, an important task is to keep low M_r (for example, the FFT step has complexity $O(M_r \log M_r)$), while satisfying the above conditions and meeting the accuracy requirements.

The minimum value of M_r satisfying Condition #3 is obtained by rewriting Eq. (1) as

$$F_k = \sum_{i=0}^{N-1} c_i e^{-j(s_k-s_b)x_i}, \tag{17}$$

with $c_i = f_i \exp(-js_b x_i)$, so that X becomes equal to $|x_b - x^{\min}| = |x^{\max} - x_b|$, with $x_b = (x^{\min} + x^{\max})/2$.

Similarly, the minimum value of M_r satisfying Condition #5 can be obtained by rewriting Eq. (17) as

$$F_k = e^{-j(s_k-s_b)x_b} \sum_{i=0}^{N-1} c_i e^{-j(s_k-s_b)(x_i-x_b)}, \tag{18}$$

so that S becomes equal to $|s_b - s^{\min}| = |s^{\max} - s_b|$, with $s_b = (s^{\min} + s^{\max})/2$.

On defining $F'_k = F_k \exp[j(s_k - s_b)x_b]$, $s'_k = (s_k - s_b)$ and $x'_i = (x_i - x_b)$, then Eq. (18) rewrites as

$$F'_k = \sum_{i=0}^{N-1} c_i e^{-js'_k x'_i}, \tag{19}$$

which is again the expression of a NUDFT-3. Henceforth, the NUFFT-3 procedure will be assumed to be applied to Eq. (19) while avoiding the primed notation and using that in Eq. (1).

4. CONDITIONS DICTATED BY THE ACCURACY

In this section, we finally deal with the choice of appropriate values for M_r, τ, σ, $2m_{sp}$, Δx and Δs satisfying the above conditions and for a fixed, desired accuracy.

In the following, we first give the assumed definition of accuracy. Later on, by exploiting the results in [15], we derive an error bound for the $\bar{F}_k$'s, $k = 1, \ldots, N_s$, when evaluated according to the Type 3 NUFFT scheme. Finally, the parameters choice is detailed.

4.1. Accuracy

Let us denote by $\|\underline{F}\|$ the ℓ^1 norm of a sequence $\underline{F} = \{F_k\}_{k=0}^{N_s-1}$ and by $\underline{\bar{F}} = \{\bar{F}_k\}_{k=0}^{N_s-1}$. Let us also define by ϵ_0 the desired accuracy and by ϵ the achieved accuracy in approximating $\underline{F}$ by $\underline{\bar{F}}$, i.e.,

$$\epsilon = \frac{\max_{k=0,\ldots,N_s-1}\{\left|F_k - \bar{F}_k\right|\}}{\|\underline{F}\|} < \epsilon_0. \tag{20}$$

On substituting Eqs. (7) and (8) in Eq. (9) and by taking into account that the Gaussian interpolation window in the spatial domain is given a bounded support determined by m_{sp}, then

$$F_\tau^{-\sigma}(m\Delta s) \simeq \frac{\Delta x}{\sqrt{2\pi}} \sum_{n'=-m_{sp}}^{m_{sp}} \left[\left(\sum_{i=0}^{N-1} \frac{1}{\sqrt{2\sigma}} e^{\sigma((\zeta_i+n')\Delta x)^2} f_i e^{-\frac{\left(\frac{x_i}{\Delta x} - (\zeta_i+n')\right)^2 \Delta x^2}{4\tau}} \right) \right] e^{-jm(\zeta_i+n')\Delta x \Delta s}. \tag{21}$$

On substituting now Eq. (21) into Eq. (10) and then the result in Eq. (11) and by taking into account that the Gaussian interpolation window in the spectral domain is given a finite support again determined by m_{sp}, we introduce

$$\bar{F}_k = \sum_{i=0}^{N-1} f_i S_{ik}, \tag{22}$$

where

$$S_{ik} = e^{b_\tau (s_k \Delta x)^2} \sum_{n'=-m_{sp}}^{m_{sp}} P_{in'} Q_{in'k}, \tag{23}$$

$$P_{in'} = \frac{1}{2\sqrt{\pi b_\tau}} e^{-\frac{\left[\frac{x_i}{\Delta x} - (\zeta_i+n')\right]^2}{4b_\tau}}, \tag{24}$$

$$b_\tau = \frac{\tau}{\Delta x^2}, \tag{25}$$

$$b_\sigma = \frac{\sigma}{\Delta s^2}, \tag{26}$$

and

$$Q_{in'k}=\frac{e^{\sigma[(\zeta_i+n')\Delta x]^2}}{2\sqrt{\pi b_\sigma}}\sum_{m'=-m_{sp}}^{m_{sp}} e^{-\frac{\left[\frac{s_k}{\Delta s}-(\eta_k+m')\right]^2}{4b\sigma}} e^{-j(\eta_k+m')(\zeta_i+n')\Delta s\Delta x}. \quad (27)$$

Let us now introduce $\bar{\bar{F}}_k$ as

$$\bar{\bar{F}}_k = \sum_{i=0}^{N-1} f_i \tilde{S}_{ik}, \quad (28)$$

where

$$\tilde{S}_{ik} = e^{b_\tau (s_k\Delta x)^2} \sum_{n'=-m_{sp}}^{m_{sp}} P_{in'} e^{-j(\zeta_i+n')s_k\Delta x}. \quad (29)$$

Both $\bar{F}_k$ and $\bar{\bar{F}}_k$ are approximations to F_k, where the first one arises from the application of the NUFFT-3 scheme, while the second one by further using the approximation

$$Q_{in'k} \simeq e^{-j(\zeta_i+n')s_k\Delta x} \quad (30)$$

which will be derived in Subsection 4.3.

In Subsection 4.5, an error bound for the approximation $F_k \simeq \bar{F}_k$ will be derived by exploiting the triangle inequality

$$\left|F_k - \bar{F}_k\right| \leq \left|\bar{\bar{F}}_k - \bar{F}_k\right| + \left|F_k - \bar{\bar{F}}_k\right| \quad (31)$$

and bounds on $|\bar{\bar{F}}_k - \bar{F}_k|$ and $|F_k - \bar{\bar{F}}_k|$. Therefore, by exploiting the procedure by Dutt and Rokhlin of [15] in Subsection 4.2, bounds for those quantities will be derived.

4.2. Corollary 2.9 of [15]

Following the procedure by Dutt and Rokhlin (Corollary 2.9 of [15]), we can express an error bound for which any function of the form e^{jcx} can be accurately represented by using a finite Fourier series with properly chosen Gaussian coefficients.

Let $b > 1/2$ and $c \neq 0$ be real numbers, and let $R \geq 2$ be an integer and $Q \geq 4\pi b$ be an even integer. Then, for any $x \in [-\pi/R, \pi/R]$

$$\left| e^{jcx} - e^{bx^2} \sum_{k=-Q/2}^{Q/2} \frac{1}{2\sqrt{\pi b}} e^{-\frac{(c-(\mathrm{Int}(c)+k))^2}{4b}} e^{j(\mathrm{Int}(c)+k)x} \right| < \delta \quad (32)$$

where

$$\delta = e^{-b\pi^2\left(1-\frac{1}{R^2}\right)}(4b+9). \quad (33)$$

4.3. Bound for $|\bar{\bar{F}}_k - \bar{F}_k|$

According to the result above, by letting $Q = 2m_{sp}$, $b = b_\sigma$, $c = s_k/\Delta s$, $R = R_1$ and $x = -(\zeta_i + n')\Delta s\Delta x$, and by noticing that $\mathrm{Int}(c) = \eta_k$, then

$$\left| e^{-j(\zeta_i+n')s_k\Delta x} - \frac{e^{\sigma[(\zeta_i+n')\Delta x]^2}}{2\sqrt{\pi b_\sigma}} \sum_{m'=-m_{sp}}^{m_{sp}} e^{-\frac{\left[\frac{s_k}{\Delta s}-(\eta_k+m')\right]^2}{4b_\sigma}} e^{-j(\eta_k+m')(\zeta_i+n')\Delta s\Delta x} \right| < \delta_1 \tag{34}$$

with

$$\delta_1 = e^{-b_\sigma\pi^2\left(1-\frac{1}{R_1^2}\right)}(4b_\sigma + 9) \tag{35}$$

which establishes the approximation (30) with an accuracy dictated by δ_1.

In the following, we report the conditions under which Eqs. (32) and (33) can be rewritten as (30), (34) and (35):

Condition #6

$$R_1 \geq 2 \tag{36}$$

Condition #7

$$\left(\frac{X}{\Delta x} + m_{sp}\right)\Delta s\Delta x \leq \frac{\pi}{R_1} \tag{37}$$

Condition #8

$$m_{sp} \geq 2\pi b_\sigma \tag{38}$$

Condition #9

$$b_\sigma \geq \frac{1}{2} \tag{39}$$

According to (34) and (35) and to the triangle inequality, then we have

$$\left|\bar{\bar{F}}_k - \bar{F}_k\right| = \left| e^{b_\tau(s_k\Delta x)^2} \sum_{i=0}^{N-1} \sum_{n'=-m_{sp}}^{m_{sp}} f_i P_{in'} \left(e^{-j(\zeta_i+n')s_k\Delta x} - Q_{in'k}\right) \right|$$

$$\leq e^{b_\tau(s_k\Delta x)^2}\delta_1 \sum_{i=0}^{N-1} |f_i| \sum_{n'=-m_{sp}}^{m_{sp}} |P_{in'}|\,. \tag{40}$$

The last inequality can be rewritten by exploiting (24) and by noticing that

$$\sum_{n'=-m_{sp}}^{m_{sp}} |P_{in'}| = \sum_{n'=-m_{sp}}^{m_{sp}} \frac{1}{2\sqrt{\pi b_\tau}} e^{-\frac{\left(\frac{x_i}{\Delta x}-(\zeta_i+n')\right)^2}{4b_\tau}}$$

$$< \sum_{n'=-\infty}^{\infty} \frac{\Delta x}{2\sqrt{\pi\tau}} e^{-\frac{\left(n'\Delta x-(x_i-\zeta_i)\Delta x\right)^2}{4\tau}}$$
$$< \int_{-\infty}^{\infty} \frac{1}{2\sqrt{\pi\tau}} e^{-\frac{\left(x-(x_i-\zeta_i)\Delta x\right)^2}{4\tau}} dx < 1 + \frac{\Delta x}{2\sqrt{\pi\tau}}. \tag{41}$$

The last inequality holds for every value of Δx and becomes tight for small values of Δx. By taking into account Eq. (25) and Condition #9, finally we have

$$\left|\bar{\bar{F}}_k - \bar{F}_k\right| < e^{b_\tau (s_k \Delta x)^2} \delta_1 \sum_{i=0}^{N-1} |f_i| \left(1 + \frac{1}{\sqrt{2\pi}}\right). \tag{42}$$

4.4. Bound for $|F_k - \bar{\bar{F}}_k|$

In this section, by exploiting again (32) and (33), we work out an approximate expression for $\tilde{S}_{ik}$, and thus for S_{ik} and $\bar{F}_k$, which will be employed to finally derive an error bound to $|F_k - \bar{\bar{F}}_k|$.

Similarly as in the previous subsection, by letting, in (32) and (33), $b = b_\tau$, $Q = 2m_{sp}$ and $c = x_i/\Delta x$, $R = R_2$ and $x = -s_k \Delta x$ and by noticing that $\mathrm{Int}(c) = \zeta_i$, we have

$$\left| e^{-j s_k x_i} - e^{b_\tau (s_k \Delta x)^2} \sum_{n'=-m_{sp}}^{m_{sp}} P_{in'} e^{-j(\zeta_i + n') s_k \Delta x} \right| < \delta_2 \tag{43}$$

with

$$\delta_2 = e^{-b_\tau \pi^2 \left(1 - \frac{1}{R_2^2}\right)} (4 b_\tau + 9). \tag{44}$$

In other words,

$$\tilde{S}_{ik} \simeq e^{-j s_k x_i}. \tag{45}$$

with an accuracy dictated by δ_2.

In the following, we report further conditions that must be satisfied to use (43), (44) and (45):

Condition #10

$$R_2 \geq 2 \tag{46}$$

Condition #11

$$S \Delta x \leq \frac{\pi}{R_2} \tag{47}$$

Condition #12

$$m_{sp} \geq 2\pi b_\tau \tag{48}$$

Condition #13

$$b_\tau \geq \frac{1}{2} \tag{49}$$

According to (43) and (44) and to the triangle inequality, then we have

$$\left|\bar{\bar{F}}_k - \bar{F}_k\right| = \left|F_k - e^{b_\tau (s_k \Delta x)^2} \sum_{i=0}^{N-1} f_i \sum_{n'=-m_{sp}}^{m_{sp}} P_{in'} e^{-j(\zeta_i + n')s_k \Delta x}\right| < \delta_2 \sum_{i=0}^{N-1} |f_i| . \tag{50}$$

4.5. Error Bound for F_k

We now finally derive an error bound for the F_k calculated according to the Type 3 NUFFT scheme.

By exploiting (31), (42) and (50) along with the triangle inequality and Condition #11, then we have

$$\left|F_k - \bar{F}_k\right| < \left[e^{b_\tau \left(\frac{\pi}{R_2}\right)^2} \delta_1 \left(1 + \frac{1}{\sqrt{2\pi}}\right) + \delta_2\right] \sum_{i=0}^{N-1} |f_i| . \tag{51}$$

Henceforth, we exploit the degrees of freedom that we have on b_τ, b_σ, R_1 and R_2 by letting

$$R = R_1 = R_2 \tag{52}$$

and

$$b = b_\tau = b_\sigma \tag{53}$$

so that $\delta_1 = \delta_2 = \delta$. Accordingly, an error bound for F_k is

$$\begin{aligned} \left|F_k - \bar{F}_k\right| &< \left|F_k - \bar{\bar{F}}_k\right| + \left|\bar{\bar{F}}_k - \bar{F}_k\right| \\ &< \delta \sum_{i=0}^{N-1} |f_i| e^{b\left(\frac{\pi}{R}\right)^2} \left[e^{-b\left(\frac{\pi}{R}\right)^2} + \left(1 + \frac{1}{\sqrt{2\pi}}\right)\right] < \delta \sum_{i=0}^{N-1} |f_i| e^{b\left(\frac{\pi}{R}\right)^2} \left[2 + \frac{1}{\sqrt{2\pi}}\right]. \end{aligned} \tag{54}$$

Therefore, the relative accuracy according to (20) is

$$\frac{\max_{k=0,\ldots,N_s-1} \left\{\left|F_k - \bar{F}_k\right|\right\}}{\|\underline{F}\|} < \epsilon(b,R) = \left(2 + \frac{1}{\sqrt{2\pi}}\right) e^{-b\pi^2\left(1 - \frac{2}{R^2}\right)} (4b+9). \tag{55}$$

5. CHOICE OF THE ALGORITHM PARAMETERS

In this section, our purpose is to select first the values of b and R so that the error bound $\epsilon(b, R)$ equals a prefixed value ϵ_0 and then determine all the other algorithm parameters according to the conditions derived above, which are summarized in Table 1.

Table 1. Summary of the general conditions and of the conditions dictated by the accuracy for the choice of the APs.

Number	Condition
1	$\sigma < 1/(4\tau)$
2	$0.5M_r \geq (X/\Delta x) + m_{sp}$
3	$\Delta x \leq \pi/B_s$
4	$\Delta s = 2\pi/(\Delta x M_r)$
5	$0.5M_r \geq (S/\Delta s) + m_{sp}$
6	$R_1 \geq 2$
7	$(X/\Delta x + m_{sp})\Delta s \Delta x \leq \pi/R_1$
8	$m_{sp} \geq 2\pi b_\sigma$
9	$b_\sigma \geq 0.5$
10	$R_2 \geq 2$
11	$S\Delta x \leq \pi/R_2$
12	$m_{sp} \geq 2\pi b_\tau$
13	$b_\tau \geq 0.5$

First of all, let us rewrite Eq. (55) as

$$b = \frac{1}{\gamma} \log \left(\frac{4\alpha}{\epsilon_0} b + \frac{9\alpha}{\epsilon_0} \right) \tag{56}$$

with

$$\alpha = 2 + \frac{1}{\sqrt{2\pi}} \tag{57}$$

and

$$\gamma = \pi^2 \left(1 - \frac{2}{R^2} \right). \tag{58}$$

This equation is transcendental and an analytical solution is not possible. However, it can be solved by "successive approximations", see Subsection 6.1. In the following, we will denote by b_n the n-th order solution to Eq. (56).

5.1. Choice of m_{sp}

The minimum value of m_{sp} needed to satisfy Conditions #8 and #12 is

$$m_{sp} = 2\pi b_n. \tag{59}$$

5.1.1. Choice of Δx and M_r

If we use Condition #4 in Condition #7, we have that

$$\frac{M_r}{2} \geq R\left(\frac{X}{\Delta x} + m_{sp}\right) \tag{60}$$

which is more restrictive than Condition #2, being $R \geq 2$ (Condition #6 and Condition #10). Furthermore, taking into account Condition #4 and Condition #11, Condition #5 rewrites as

$$M_r \geq \frac{2R}{R-1} m_{sp}. \tag{61}$$

Then, M_r should meet the most stringent between (60) and (61). However, $R/(R-1) \leq 2$ when $R \geq 2$, so that (61) implies that $M_r \geq 4m_{sp}$ at most. Since we expect that $X/\Delta x \gg m_{sp}$ so that $M_r \gg m_{sp}$, then we can stipulate that M_r must satisfy the inequality (60) only. In order to keep low the value of M_r, then we choose the maximum possible value for Δx according to Condition #11, i.e.,

$$\Delta x = \frac{\pi}{RS}. \tag{62}$$

The consequent choice of M_r is

$$M_r \geq 2\left(\frac{XSR^2}{\pi} + 2\pi R b_n\right). \tag{63}$$

Note that the expression for M_r is parameterized to R. In order to reduce the computational complexity of the algorithm, we are obviously interested to choose the value of R yielding the minimum value for M_r, while satisfying the required accuracy. To this end, we notice that the first term of the right hand side of (63), which is much larger than the second one, grows as R^2 so that it achieves its minimum value for $R = 2$ when taking into account that Conditions #6 and #10 imply $R \geq 2$. Therefore we henceforth choose R slightly larger than 2.

Up to now, we have exploited all the above Conditions, except for Conditions #1 and #3, and we have set the parameters m_{sp}, b, Δx and M_r. In the next subsection we will deal with the choice of Δs, τ and σ.

5.2. Choices of Δs, τ and σ

The parameter Δs is set according to Eq. (15). The parameters τ and σ can be straightforwardly determined from Eqs. (25) and (26). It remains to check Conditions #1 and #3.

Let us verify first Condition #1. To this end, we notice that, from Condition #4 and from Eqs. (25) and (26),

$$\frac{1}{4\tau} - \sigma = b\Delta s^2 \left[\left(\frac{M_r}{2m_{sp}} \right)^2 - 1 \right] > 0, \tag{64}$$

since we expect that, as we noticed in Subsection 5.1.1, $M_r \gg m_{sp}$, so that Condition #1 is met.

Finally, and concerning Condition #3, determining B_s requires determining the support of $F_\tau^{-\sigma}(s)$. To this end, we observe that $F_\tau^{-\sigma}(s)$ can be rewritten as

$$F_\tau^{-\sigma}(s) = \frac{1}{\sqrt{4\pi\sigma}} \sum_{j=0}^{N-1} f_j I_j(s), \tag{65}$$

with

$$I_j(s) = \int_{-\infty}^{\infty} e^{\sigma x^2} e^{-\frac{(x-x_j)^2}{4\tau}} e^{-jsx} dx = e^{-\frac{s^2}{4d}} \sqrt{\frac{\pi}{d}} e^{-\frac{x_j^2}{4\tau}\left(1+\frac{1}{4d\tau}\right)} e^{\frac{x_j s}{4d\tau}}, \tag{66}$$

and

$$d = \left(\frac{1}{4\tau} - \sigma \right). \tag{67}$$

In other words,

$$F_\tau^{-\sigma}(s) = \frac{1}{\sqrt{4\pi\sigma}} \sqrt{\frac{\pi}{d}} e^{-\frac{s^2}{4d}} \sum_{j=0}^{N-1} f'_j e^{\frac{x_j s}{4d\tau}}, \tag{68}$$

where

$$f'_j = f_j e^{-\frac{x_j^2}{4\tau}\left(1+\frac{1}{4d\tau}\right)} \quad j = 1, \ldots, N. \tag{69}$$

According to (68), the bandwidth of $F_\tau^{-\sigma}(s)$ is essentially limited by the support of the Gaussian function $\exp(-(s^2/(4d))$. Defining the support of $\exp(-(s^2/(4d))$ by the value of $s = B_s$ guaranteeing that

$$e^{-\frac{B_s^2}{4d}} = \epsilon_k \ll 1, \tag{70}$$

then

$$B_s = 2\sqrt{\log\left(\frac{1}{\epsilon_k}\right)} \sqrt{\frac{M_r^2}{16b\pi^2} - b}. \tag{71}$$

We have verified that, for the numerical cases of next section, Condition #3 is satisfied when $\epsilon_k = 10^{-5}$.

6. NUMERICAL RESULTS

We now present numerical outcomes aiming at proving how the parameters choice according to the developed procedure returns consistent results. Before showing the numerical results in Subsection 6.2, in the next subsection we detail the numerical solution of Eq. (56). Lastly, in Subsection 6.3, the main issues of the approach in [2] are highlighted.

6.1. Successive Approximation Solution to Eq. (56)

Let us begin by observing that the function

$$h(b) = \frac{1}{\gamma} \log\left(\frac{4\alpha b}{\epsilon_0} + \frac{9\alpha}{\epsilon_0}\right) \tag{72}$$

is a contraction [21]. Indeed, by enforcing that $|h'(b)| < 1$, we obtain the condition

$$b \geq \left(\frac{1}{\gamma} - \frac{9}{4}\right). \tag{73}$$

Since the minimum value of γ is achieved for $R = 2$, then Condition #9 and Condition #13 are more restrictive than (73) and so $|h'(b)| < 1$ is met, $h(b)$ is a contraction according to Lagrange's theorem and the solution to Eq. (56) is unique. Setting $b > 0.5$ and taking into account that the minimum value of γ equals $\pi^2/2$, the contraction constant is $K = 8/(11\pi^2)$.

Since $h(b)$ is a contraction, then, according to the Banach-Caccioppoli theorem, Eq. (56) can be solved by a successive approximation procedure in which the solution b_n at the n-th iteration is

$$b_n = h(b_{n-1}), \tag{74}$$

and b_0 is arbitrarily chosen.

The sequence $\{b_n\}$ in Eq. (74) is convergent and

$$\left|b_n - \bar{b}\right| \leq \frac{|b_0 - b_1|}{1 - K} K^n, \tag{75}$$

where b_1 is the first-order solutions and $\bar{b}$ is the solution to (74), provides an error estimate as well as the number of iterations required to reach the solution.

By setting $b_0 = 0.5$, for the case $\epsilon_0 = 10^{-11}$ and $R = 2$, the solution is reached in 4 iterations with an error, given by (75), equal to 10^{-4}. When necessary, the convergence can be expedited by means of the Aitken extrapolation scheme [22].

6.2. Results

First of all, let us summarize that the algorithm parameters are selected according to the following steps:

(i) A desired accuracy ϵ_0 is selected. ϵ_0 is the value that we desire our definition of relative accuracy ϵ is less than. If, for example, we select $\epsilon_0 = 10^{-11}$ and for a proper choice of the algorithm parameters, the condition

$$\epsilon < 10^{-11} \tag{76}$$

must be verified.

(ii) R is chosen just slightly larger than the limiting case 2, $R = 2.1$ in the following, according to Conditions #6 and #10 and to the discussion in Subsubsection 5.1.1.

(iii) b is chosen according to the successive approximations of Eq. (56) detailed in foregoing subsection. Throughout the numerical analysis and without any loss of generality, the first order approximation

$$b = -\frac{R^2 \log\left(\frac{\epsilon_0}{11\alpha}\right)}{\pi^2 \left(R^2 - 2\right)} \tag{77}$$

has been employed.

(iv) m_{sp} is chosen according to $m_{sp} = 2\pi b$, see the beginning of Subsection 5.1.

(v) For fixed values of X and S, M_r is chosen as

$$M_r = 2\left[\frac{XS}{\pi}R^2 + Rm_{sp}\right] \tag{78}$$

according to Eq. (63).

(vi) Δx is chosen as

$$\Delta x = \frac{\pi}{RS} \tag{79}$$

according to Eq. (62)

(vii) Δs is chosen as

$$\Delta s = \frac{2\pi}{\Delta x M_r} \tag{80}$$

according to Eq. (15).

(viii) τ is chosen as

$$\tau = \Delta x^2 b \tag{81}$$

according to Eqs. (25) and (53).

(ix) σ is chosen as

$$\sigma = \Delta s^2 b \tag{82}$$

according to Eqs. (26) and (53).

The parameters choice is summarized in Table 2.

Table 2. Summary of the choice of the APs.

b chosen according to successive approximations of Eq. (56)
$m_{sp} = 2\pi b$
$\Delta x = \frac{\pi}{RS}$
$\Delta s = \frac{2\pi}{\Delta x M_r}$
$M_r \geq 2\left(\frac{XSR^2}{\pi} + 2\pi R b_n\right)$
$\tau = b\Delta x^2$
$\sigma = b\Delta s^2$

After the parameters selection, to enable a statistical numerical analysis, test-case values for X and S are fixed and N non-uniformly spaced, random points with uniform distribution within the intervals $[-X, X]$ and $[-S, S]$ are generated, for a fixed N. Furthermore, random complex values for f_i with uniformly distributed real and imaginary parts are generated. The NUFFT-3 algorithm is then applied and the results $\bar{F}_k$'s are compared to the "exact" values F_k's of Eq. (1) by calculating ϵ.

In Fig. 1, we illustrate the choice of M_r for different values of X and S and for $\epsilon_0 = 10^{-11}$ and in Table 3 we indicate the choices of

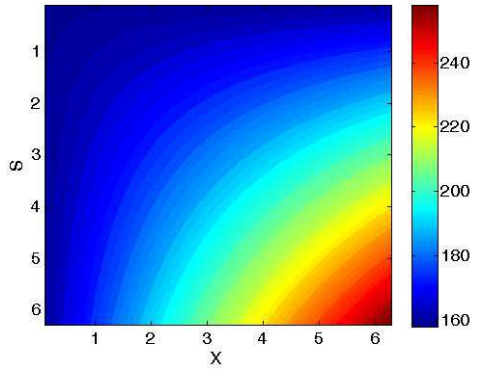

Figure 1. Choices of M_r for different values of X and S and for $\epsilon_0 = 10^{-11}$.

Table 3. Choices of m_{sp} for different values of ϵ_0.

ϵ_0	m_{sp}
10^{-7}	25
10^{-8}	28
10^{-9}	31
10^{-10}	33
10^{-11}	36
10^{-12}	39

m_{sp}, which is independent on X and S, for different values of ϵ_0.

Concerning the accuracy (according to the definition in Eq. (20)), in Figs. 2, 3 and 4 the case is considered when $X = 2\pi$ and $S = 2\pi$ and the required accuracy is $\epsilon_0 = 10^{-10}$, $\epsilon_0 = 10^{-11}$ and $\epsilon_0 = 10^{-12}$, respectively. As can be seen, the accuracy meets the requirements for all the considered 25 realizations. We can also observe that the actual accuracy is much better than the required one. This is due to the fact, recognized in [20], that the bound in Corollary 2.9 of [15] is somewhat weak, leading to actual accuracies much better than those foreseen.

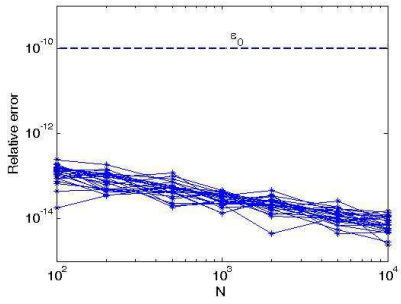

Figure 2. Log-log relative error, according to (20), for $X = 2\pi$, $S = 2\pi$, $\epsilon_0 = 10^{-10}$, for different values of N and for 25 runs.

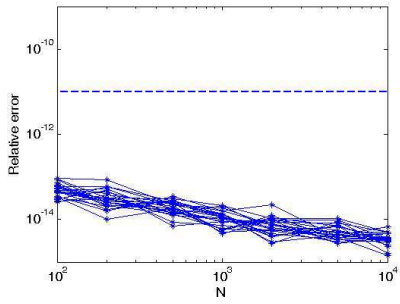

Figure 3. Log-log relative error, according to (20), for $X = 2\pi$, $S = 2\pi$, $\epsilon_0 = 10^{-11}$, for different values of N and for 25 runs.

6.3. Parameters Choice of [2]

We finally briefly sketch how the parameters choice in [2] leads to inconsistent results. The main problems with the approach in [2] are that the parameter choice is actually lacking, the function $f_\tau^{-\sigma}(x)$ has

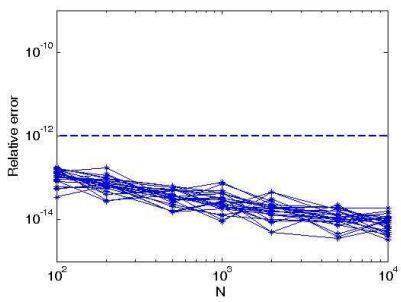

Figure 4. Log-log relative error, according to (20), for $X = 2\pi$, $S = 2\pi$, $\epsilon = 10^{-12}$, for different values of N and for 25 runs.

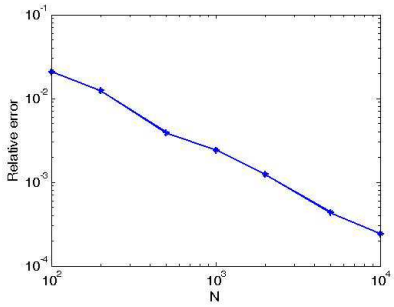

Figure 5. Log-log scale, accuracy result for the approach in [2] when $X = 2\pi$ and $S = 2\pi$.

a non-finite support and the parameter choice is independent of the requested accuracy, as opposed to our approach.

First, we summarize the parameters selection

$$\Delta x \leq \frac{\pi}{S}\frac{1}{R}, \tag{83}$$

$$\Delta s \leq \frac{\pi}{X + m_{sp}\Delta x}\frac{1}{R}, \tag{84}$$

$$\tau \simeq \frac{\Delta x}{2\pi}\frac{m_{sp}}{R(R-1)}, \tag{85}$$

$$\sigma \simeq \frac{\Delta s}{2\pi}\frac{m_{sp}}{R(R-1)}, \tag{86}$$

and

$$M_r = \frac{2\pi}{\Delta x \Delta s}, \tag{87}$$

with $R = \sqrt{2}$ [2]. Note that the above parameters choice is independent on the targeted accuracy. The Authors suggest a value of m_{sp} equal to 18 to achieve twelve digits of accuracy, so we fix $m_{sp} = 18$. Furthermore, they do not enforce Condition #1. Consequently, if we consider the above Conditions as equalities (which is an admissible possibility) then the function $f_\tau^{-\sigma}(x)$ has a non-finite support and becomes numerically untractable.

On the other side, by enforcing Condition #1, then

$$M_r \geq \frac{2m_{sp}^2}{\pi R^2 (R-1)^2}. \tag{88}$$

Considering the example of Subsection 6.2 with $X = 2\pi$ and $S = 2\pi$ and the equality sign in (88) so that $M_r = 852$, let us choose

$$\Delta x = 0.001 \frac{\pi}{S} \frac{1}{R}, \tag{89}$$

$$\Delta 2 = \frac{2\pi}{\Delta x M_r}, \tag{90}$$

$$\tau = 0.9 \frac{\Delta x}{2\pi} \frac{m_{sp}}{R(R-1)}, \tag{91}$$

and

$$\sigma = 0.9 \frac{\Delta s}{2\pi} \frac{m_{sp}}{R(R-1)}. \tag{92}$$

The accuracy result (according to (55)) is reported in Fig. 5. As can be seen, the achieved accuracy is very poor.

7. ELECTROMAGNETIC APPLICATION

In this section, we show that the aggregation and disaggregation stages of the FMM can be effectively performed by a NUFFT-3 [7]. Without loss of generality, we here focus the attention on the 2D Electric Field Integral Equation (EFIE) for the case of a perfectly conducting cylinder under TM (Transverse Magnetic) illumination.

Let us then consider the perfectly conducting cylinder, embedded in free-space, with contour C illustrated in Fig. 6. The incident field $E_z^{inc}(\underline{\rho})$ excites a surface current density $J_z(\underline{\rho})$ on C, so that the EFIE is written as [23]

$$E_z^{inc}(\underline{\rho}) = \frac{\omega\mu_0}{4} \int_C J_z(\underline{\rho}') H_0^{(2)} \left(k_0 \left|\underline{\rho} - \underline{\rho}'\right|\right) dC, \quad \underline{\rho} \in C, \tag{93}$$

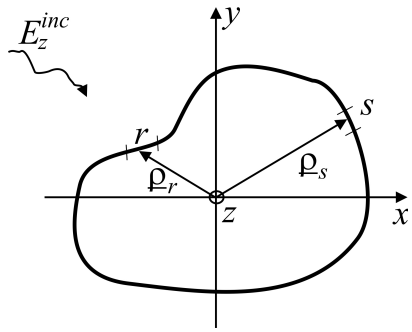

Figure 6. Geometry of the FMM problem.

where μ_0 is the free-space permeability, λ_0 the free-space wavelength, $k_0 = 2\pi/\lambda_0$, and $H_0^{(2)}(\cdot)$ the zero-th order Hankel function of the second kind.

The EFIE is here discretized by dividing the contour C into N segments of width w_s, $s = 1, \ldots, N$, and by approximating the current J_z as constant over each segment and equal to I_s. For the sake of simplicity, we approximate the integral in Eq. (93) over each segment by a simple one-point integration rule [24] and enforce Eq. (93) at the centers $\underline{\rho}_r$ of each segment. Consequently, Eq. (93) can be rewritten as

$$\underline{V} = \underline{\underline{Z}}\, \underline{I}, \tag{94}$$

where

$$V_r = E_z^{inc}(\underline{\rho}_r), \tag{95}$$

$$Z_{rs} = \begin{cases} \frac{\omega\mu_0}{4} w_s \left[1 - j\frac{2}{\pi}\log\left(\frac{\gamma k_0 w_s}{4e}\right)\right] & r = s \\ \frac{\omega\mu_0}{4} w_s H_0^{(2)}(k_0\rho_{rs}) & r \neq s \end{cases}, \tag{96}$$

$\gamma = 1.718$ is the Euler's constant and $\rho_{rs} = |\underline{\rho}_r - \underline{\rho}_s|$. In (96), the integration for the self-term (i.e., $r = s$) has been performed by approximating the Hankel function for small arguments [23].

The $O(N^2)$ cost for evaluating Eq. (94) can be mitigated by associating the segments into M groups and by identifying, for each segment r of a certain group G_m, two contributions: one related to the near-field, i.e., to other segments s "near" to r, and one to the far-field interactions due to the "far" groups G_n. In other words,

$$V_r = \sum_{s \text{ "near" to } r} Z_{rs} I_s + \sum_{G_s \text{ "far" to } r} \sum_{s \in G_n} Z_{rs} I_s, \quad r \in G_m. \tag{97}$$

The first summation in Eq. (97) regards the near-field interactions, and involves all the "source" segments s belonging to the groups "near" to the "observation" segment r. On the other side, the second summation in Eq. (97) concerns the far-field interactions, and involves all the "source" segments belonging to the groups G_n which are "far" from the segment r. The FMM simplifies the calculation of the second contribution. Indeed, consider the relation

$$H_0^{(2)}(k_0\rho_{rs}) \simeq \frac{1}{2\pi}\int_0^{2\pi} e^{-jk_0\rho_{rm}\cos(\alpha-\phi_{rm})} a_{mn}(\alpha) e^{-jk_0\rho_{nm}\cos(\alpha-\phi_{ns})} d\alpha \tag{98}$$

where m and n denote the groups containing the segments r and s, respectively, and $\underline{\rho}_n - \underline{\rho}_s = (\rho_{ns}\cos\phi_{ns}, \rho_{ns}\sin\phi_{ns})$, $\underline{\rho}_m - \underline{\rho}_r = (\rho_{mr}\cos\phi_{mr}, \rho_{mr}\sin\phi_{mr})$, $\underline{\rho}_m$ and $\underline{\rho}_n$ are the "group centers" of groups

m and n, and

$$a_{mn}(\alpha) = \sum_{l=-L}^{L} H_l^{(2)}(k_0\rho_{mn}) e^{-jl\left(\phi_{mn}-\alpha+\frac{\pi}{2}\right)}, \tag{99}$$

with $\underline{\rho}_m - \underline{\rho}_n = (\rho_{mn}\cos\phi_{mn}, \rho_{mn}\sin\phi_{mn})$. A value of L leading to a good approximation of Eq. (98) is given by $L = k_0R + K'(k_0R)$, where R is the radius of the minimum circle containing each group, $K' = 1.8(d_0)^{2/3}$ and d_0 is the number of digits of accuracy [25].

On discretizing Eq. (98) by a uniform sampling in the α variable, then the far-field interactions of Eq. (97) can be rewritten, apart from the factor $(w_s\Delta\alpha\omega\mu_0)/(8\pi)$, as

$$\underbrace{\sum_k e^{-jk_0\rho_{rm}\cos(\alpha_k-\phi_{\phi_{rm}})} \underbrace{\sum_{G_n} a_{mn}(\alpha_k) \underbrace{\sum_{s\in G_n} e^{-jk_0\rho_{ns}\cos(\alpha_k-\phi_{ns})} I_s}_{\text{Aggregation } (A)}}_{\text{Translation } (T)}}_{\text{Disaggregation } (D)}, \quad r \in G_m. \tag{100}$$

where $\Delta\alpha$ is the sampling step in α. In Eq. (100), the aggregation, translation and disaggregation steps are highlighted.

Let us now point out how the aggregation and disaggregation steps of Eq. (100) can be performed by a NUFFT-3.

Let us consider the aggregation step first. The aggregation term (A) in Eq. (100) can be rewritten as

$$(A) = \sum_{s\in G_n} e^{-jk_0[(x_n-x_s)\cos\alpha_k+(y_n-y_s)\sin\alpha_k]} I_s. \tag{101}$$

As can be seen and for a fixed n, Eq. (101) is the expression of a 2D DFT from the non-uniform spatial grid $(x_n - x_s,\, y_n - y_s)$ to the spectral grid $(k_0\cos\alpha_k,\, k_0\sin\alpha_k)$ which arises to be non-uniform being the α_k's uniformly sampled. Accordingly, the calculations in (101) can be performed by a NUFFT-3.

Concerning now the disaggregation step, on letting

$$B_{mk} = \sum_{G_n} a_{mn}(\alpha_k) \sum_{s\in G_n} e^{-jk_0\rho_{ns}\cos(\alpha_k-\phi_{ns})} I_s, \tag{102}$$

the Eq. (100) can be rewritten as

$$D = \sum_k e^{-jk_0[(x_r-x_m)\cos\alpha_k+(y_r-y_m)\sin\alpha_k]} B_{mk}. \tag{103}$$

As can be seen and for a fixed m, Eq. (103) is the expression of a 2D DFT from the non-uniform spatial grid $(x_r - x_m,\, y_r - y_m)$ to

the non-uniform spectral grid $(k_0 \cos\alpha_k,\ k_0 \sin\alpha_k)$. Accordingly, once again, the calculations in (103) can be performed by a NUFFT-3.

We finally analyze the accuracy of using the NUFFT-3 algorithm with reference to the canonical case of a circular, perfectly conducting cylinder having radius $r = 3\lambda_0$. The cylinder's surface has been discretized in 1536 segments, grouped in 32 clusters [24]. Figs. 7 and 8 show the scattered field on the cylinder's surface as evaluated according to the far-field interactions only. In order words, for each

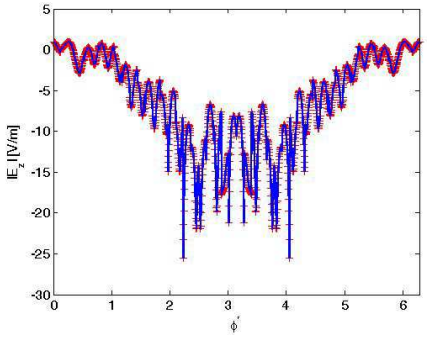

Figure 7. Scattered field amplitude on the cylinder's surface concerning the far-field interactions only. Aggregation and disaggregation evaluated in an exact way (blue line) and evaluated by a type-3 NUFFT (red crosses).

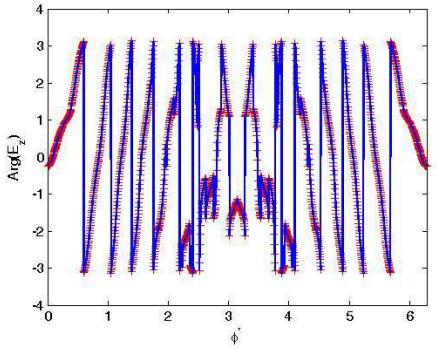

Figure 8. Scattered field phase on the cylinder's surface concerning the far-field interactions only. Aggregation and disaggregation evaluated in an exact way (blue line) and evaluated by a type-3 NUFFT (red crosses).

surface segment, the only second term in Eq. (97) is considered. More in detail, we compare the cases when aggregation and disaggregation are evaluated in an exact way and by a NUFFT-3. The good accuracy of the NUFFT-based version is witnessed by the very low relative root mean square error between the two compared cases and equal to $9.64 \cdot 10^{-11}$. Note that the accuracy of using the NUFFT-3 could have been also shown by comparing the results of a "standard" FMM-based inversion of Eq. (93) and an FMM inversion thereof using the NUFFT-3 algorithm. However, this has been avoided since the reconstructed surface current densities would have been also affected by numerical inversion errors.

8. CONCLUSIONS

We have proposed a parameters' choice for the Type 3 Non-Uniform Fast Fourier Transform (NUFFT-3) algorithm based on the Gaussian gridding.

Appropriate conditions to be satisfied by the algorithm parameters to meet a desired accuracy level have been derived by exploiting also the results in [15]. A strategy to choose the NUFFT-3 parameters has been devised to meet such conditions. For the Reader's convenience, the choice of the algorithm parameters is summarized in Table 2. We have shown how the proposed choice ensures a particularly desired accuracy in the one dimensional case. It has been also shown how the parameters choice of [2] leads to inconsistent or poorer results. Finally, the use of the NUFFT-3 has been highlighted for an electromagnetic application consisting of the implementation of the aggregation and disaggregation steps in the fast calculation of the scattered field by the Fast Multipole Method.

ACKNOWLEDGMENT

This work was partially funded by the Italian Ministry of Education, University and Research (MIUR) within the framework of project PON01_02425 "Services for Wireless Network Infrastructure beyond 3G" (SIRIO).

REFERENCES

1. Bronstein, M., A. Bronstein, and M. Zibulevsky, "The non-uniform FFT and its applications," Technical Report of the Vision and Image Science Laboratory, Israel Institute of Technology, Technion, 2002.

2. Lee, J.-Y. and L. Greengard, "The type 3 nonuniform FFT and its applications," *J. Comput. Phys.*, Vol. 206, No. 1, 1–5, Jun. 2005.
3. Capozzoli, A., C. Curcio, and A. Liseno, "GPU-based ω-k tomographic processing by 1D non-uniform FFTs," *Progress In Electromagnetics Research M*, Vol. 23, 279–298, 2012.
4. Liu, Q. H., X. M. Xu, B. Tian, and Z. Q. Zhang, "Applications of nonuniform fast transform algorithms in numerical solutions of differential and integral equations," *IEEE Trans. Geosci. Remote Sens.*, Vol. 38, No. 4, 1551–1560, Jul. 2000.
5. Li, J.-R., D. Calhoun, and L. Brush, "Efficient thermal field computation in phase-field models," *J. Comput. Phys.*, Vol. 228, No. 24, 8945–8957, Dec. 2009.
6. Bakır, O., H. Bağcı, and E. Michielssen, "Adaptive integral method with fast Gaussian gridding for solving combined field integral equations," *Waves Random Media*, Vol. 19, No. 1, 147–161, Feb. 2009.
7. Capozzoli, A., C. Curcio, and A. Liseno, "2D fast multipole method (FMM) via type-3 non-uniform FFTs (NUFFTs)," *Proc. of the Loughborough Conf. on Antennas Prop.*, 1–4, Loughborough, UK, Nov. 12–13, 2012,
8. Capozzoli, A., C. Curcio, G. D'Elia, A. Liseno, and P. Vinetti, "Fast CPU/GPU pattern evaluation of irregular arrays," *Applied Comput. Electromagn. Soc. J.*, Vol. 25, No. 4, 355–372, Apr. 2010.
9. Capozzoli, A., C. Curcio, A. Liseno, and G. Toso, "Phase-only synthesis of flat aperiodic reflectarrays," *Progress In Electromagnetics Research*, Vol. 133, 53–89, 2013.
10. Capozzoli, A., C. Curcio, and A. Liseno, "NUFFT-accelerated plane-polar (also phaseless) near-field/far-field transformation," *Progress In Electromagnetics Research M*, Vol. 27, 59–73, 2012.
11. Bronstein, M. M., A. M. Bronstein, M. Zibulevsky, and H. Azhari, "Reconstruction in diffraction ultrasound tomography using nonuniform FFT," *IEEE Trans. Medical Imaging*, Vol. 21, No. 11, 1395–1401, Nov. 2002.
12. Zhang-O'Connor, Y. and J. A. Fessler, "Fourier-based forward and back-projectors in iterative fan-beam tomographic image reconstruction," *IEEE Trans. Medical Imaging*, Vol. 25, No. 5, 582–589, May 2006.
13. Matej, S., J. A. Fessler, and I. G. Kazantsev, "Iterative tomographic image reconstruction using Fourier-based forward and back-projectors," *IEEE Trans. Medical Imaging*, Vol. 23, No. 4, 401–412, Apr. 2004.

14. Eggers, H., T. Knopp, and D. Potts, "Field inhomogeneity correction based on gridding reconstruction for magnetic resonance imaging," *IEEE Trans. Medical Imaging*, Vol. 26, No. 3, 374–384, Mar. 2007.
15. Dutt, A. and V. Rokhlin, "Fast Fourier transforms for nonequispaced data," *SIAM J. Sci. Comp.*, Vol. 14, No. 6, 1368–1393, 1993.
16. Potts, D., G. Steidl, and M. Tasche, "Fast Fourier transforms for nonequispaced data: A tutorial," *Modern Sampling Theory: Mathematics and Application*, 253–274, J. J. B. P. Ferreira, Ed., Birkhauser, Boston, MA, 2000.
17. Fessler, J. A. and B. P. Sutton, "Nonuniform fast Fourier transforms using min-max interpolation," *IEEE Trans. Signal Proc.*, Vol. 51, No. 2, 560–574, Feb. 2003.
18. Fourmont, K., "Non-equispaced fast Fourier transforms with applications to tomography," *J. Fourier Anal. Appl.*, Vol. 9, No. 5, 431–450, 2003.
19. Greengard, K. and J.-Y. Lee, "Accelerating the nonuniform fast Fourier transform," *SIAM Rev.*, Vol. 46, No. 3, 443–454, 2004.
20. Dutt, A., "Fast Fourier transforms for nonequispaced data," Ph.D. Dissertation, Yale University, YALEU/CSD/RR #981, 1993.
21. Kantorovich, L. V. and G. P. Akilov, *Functional Analysis*, Pergamon Press, New York, 1982.
22. Pozrikidis, C., *Numerical Computation in Science and Engineering*, Oxford University Press, Oxford, 2008.
23. Morita, N., "The boundary-element method," *Analysis Methods for Electromagnetic Wave Problems*, E. Yamashita (ed.), Artech House, Norwood, MA, 1990.
24. Chew, W. C., J.-M. Jin, E. Michielssen, and J. Song, *Fast and Efficient Algorithms in Computational Electromagnetics*, Artech House, Norwood, MA, 2001.
25. Song, J. and W. C. Chew, "Error analysis for the truncation of multipole expansion of vector's Green's functions," *Microw. Opt. Tech. Lett.*, Vol. 11, No. 7, 311–313, Jul. 2001.